THE JOURNAL OF PHYSICAL CHEMISTRY B

Article

pubs.acs.org/JPCB

Hydrodynamic Size-Dependent Cellular Uptake of Aqueous QDs Probed by Fluorescence Correlation Spectroscopy

Chaoqing Dong and Joseph Irudayaraj*

Department of Agricultural and Biological Engineering, Bindley Bioscience Center and Birck Nanotechnology Center, Purdue University, West Lafayette, Indiana 47907, United States

Supporting Information

ABSTRACT: Aqueous quantum dots (QDs) directly synthesized with various thiol ligands have been investigated as imaging probes in living cells. However, the effect of the surface chemistry of these ligands on QDs' cellular uptakes and their intracellular fate remains poorly understood. In this work, four CdTe QDs were directly synthesized under aqueous conditions using four different thiols as stabilizers and their interactions with cells were investigated. Fluorescence correlation spectroscopy (FCS), X-ray photoelectron spectroscopy (XPS), and zeta potential measurements on QDs primarily show that the surface structure of these QDs is highly dependent on the thiol ligands used in the preparation of QDs' precursors, including its layer thicknesses, densities, and surface charges. Subsequently, FCS integrated with the maximum-entropy-method-based FCS (MEMFCS) was used to investigate the concentration distribution and dynamics of these QDs in living A-427 cells. Our findings indicate that QDs' surface characteristics affect cell membrane adsorption and subsequent internalization. More critically, we show that the cellular uptake of aqueous QDs is dependent on their hydrodynamic diameter and might have the potential to escape trapped environments to accumulate in the cytoplasm.

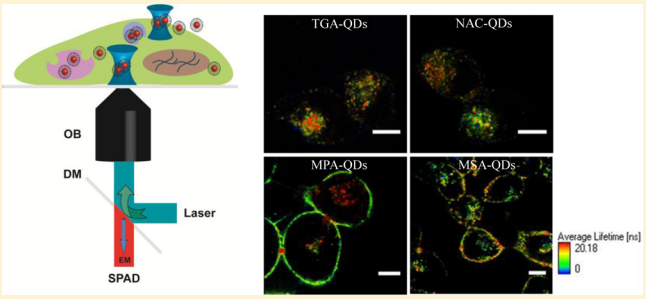

1. INTRODUCTION

There has been a growing interest in utilizing luminescent quantum dots (QDs) for biological and medical applications including *in vivo* imaging[1−4] and photodynamic therapy.[5,6] The versatility of QDs arises from their unique size-dependent photoluminescent (PL) emission spectra and fascinating optical properties such as high PL quantum yields (QYs), good chemical and photostability, etc. Studies on the cellular uptake and intracellular fate of QDs indicate that the interaction of QDs with cells is influenced by many factors, such as size, surface charge, and even the type of cells.[7−10] In order to reach their full potential with respect to intracellular applications, quantitative and qualitative methods that can provide information on cellular interaction, uptake, and localization in subcellular compartments and cytotoxicity must be developed. Luminescent aqueous QDs have much smaller hydrodynamic diameters (less than 10 nm) than their commercial counterparts synthesized in the organic phase and modified with amphiphilic polymer.[11] The reduced size and particular surface structure formed during the synthesis is assumed to result in different interactions with the cells, that influence cellular uptake and intracellular fate. However, to date, the cellular uptake mechanism of unconjugated aqueous QDs is largely unknown.[12−14]

Previous studies on the uptake of nanoparticles such as gold nanoparticles have focused on a few off-line techniques and not in living cells. For example, transmission electron microscopy (TEM) has been used to record high-resolution images of nanoparticles in cells. Inductively coupled plasma atomic emission spectroscopy (ICP-AES) and inductively coupled plasma mass spectroscopy (ICP-MS) techniques have been used to measure the concentration of Au and the number of gold nanoparticles in cells.[15−17] These methods also provide a measure of the total molar amount of QDs uptaken by cells.[18] However, TEM- and ICP-based methods are complex and time-consuming and not applicable for live cell studies. Confocal fluorescence imaging analysis has been used to visualize the uptake process of QDs and their fate within the cell. However, a quantitative evaluation of QD uptake by cells is challenging with conventional fluorescence intensity measurements and images primarily because of the lack of standards between the fluorescence intensity and the concentration. First, as reported, the brightness per particle (BPP) of QDs increases with size.[19] Second, BPP values for QDs with different thiol-capping are remarkably different, although their PL emission wavelengths are almost identical, as indicated in Figure S-1 (Supporting Information). Third, upon internalization, their fluorescence seemed to vary. For example, the fluorescence of QDs could be partly quenched by small molecules in cells. A

Received: June 6, 2012
Revised: September 4, 2012
Published: September 5, 2012

decrease in fluorescence is also possible because of the energy transfer between QDs and conjugated biomacromolecules.[12]

Fluorescence correlation spectroscopy (FCS) is an ultrasensitive and noninvasive single molecule detection technique that monitors the fluorescence fluctuations of diffusers from a small observation volume in a diffraction limited spot.[20−24] FCS may offer exciting perspectives in studying and monitoring the dynamics of targeting nanoparticles in cells.[25−27] In this work, in order to study the cellular uptake of aqueous QDs, CdTe QDs were directly synthesized using four different ligands as stabilizers under aqueous conditions, without any ligand-exchanged procedures. The four different surface ligands are thioglycolic acid (TGA), mercaptopropionic acid (MPA), mercaptosuccinic acid (MSA), and *N*-acetyl-L-cysteine (NAC). When FCS along with other techniques were used to investigate the surface structure, we noted that the surface of QDs can be remarkably influenced by the surface ligands, such as hydrodynamic diameter, surface zeta potential, and ligand density. Enlightened by these phenomena, we investigated the possible effect of surface characteristics on the cellular uptake of aqueous QDs. A-427 cells (HTB-53, Manassas, VA) were chosen as the model system to study the interaction of QDs. The cellular uptake of four QDs was quantitatively evaluated for their concentration, membrane dynamics, and cytoplasmic localization using FCS and MEMFCS. Our results show that the uptake of aqueous QDs is highly surface dependent and has the potential to escape from trapped environments and accumulate in the cytoplasm.

2. MATERIALS AND METHODS

2.1. Materials. All chemicals used in our experiments were of the highest purity available commercially. Thioglycolic acid (TGA), mercaptopropionic acid (MPA), mercaptosuccinic acid (MSA), *N*-acetyl-L-cysteine (NAC), $CdCl_2 \cdot 2.5H_2O$ (99%), and bovine serum albumin (BSA) were acquired from Sigma-Aldrich Co. (St. Louis, MO). Tellurium powder (~60 mesh, 99.999%) and sodium borohydride (98+%) were obtained from Alfa Aesar (Ward Hill, MA). Rhodamine 6G (R6G) and rhodamine 123 were purchased from Molecular Probes (Eugene, Oregon). The Amicon Ultra centrifugal filter unit (ultracel-10K, 10 000 MWCO) was from Millipore Co. (Billerica, MA).

2.2. Synthesis of Aqueous CdTe QDs. All aqueous CdTe QDs were directly prepared through a similar method except that different thiol ligands were used and the pH of their Cd precursor was adjusted to an optimized value.[28,29] The method for MPA-capped QDs is provided below as an example. Briefly, Cd precursor solutions were prepared by mixing a solution of $CdCl_2$ in the presence of thiol (MPA), and were then adjusted to a pH of 8.0 with 1 M NaOH and the solution deaerated with N_2 for 30 min. Under vigorous stirring, the oxygen-free NaHTe solution was prepared according to the reference and introduced.[28] A typical molar ratio of Cd^{2+}:NaHTe:MPA was kept at 1:0.2:2.5 in our experiments (Cd^{2+} = 2 mM). The mixture was then heated in a 95 °C water bath and reacted for a duration depending upon the size. QDs with different emission wavelengths were obtained from the reaction stock at different reaction times.

The optimized pH values of their Cd precursor were 7.0 for MSA-capped QDs, 9.5 for NAC-capped QDs, and 11.5 for TGA-capped QDs, respectively. The molar ratio of Cd^{2+}:NaHTe:MSA/NAC was 1:0.2:2.5 (Cd^{2+} = 2 mM) for MSA-capped and NAC-capped QDs, and that of Cd^{2+}:NaHTe:TGA was 1:0.2:1.2 for TGA-capped QDs in our experiments (Cd^{2+} = 10 mM). Before QDs were incubated with cells, raw QDs were purified three times with an Amicon Ultra centrifugal filter unit (ultracel-10K, 10 000 MWCO) to remove the free Cd precursor.

2.3. Characterization of CdTe QDs. UV−vis absorption spectra of CdTe QDs were measured using a Jasco V570 UV/visible/NIR spectrophotometer (Easton, MD). Samples were prepared by diluting CdTe QD solutions with ultrapure water. Photoluminescence spectra were recorded by a Cary Eclipse Fluorescence Spectrophotometer (Varian). All optical measurements were carried out at room temperature. The quantum yield (QY) of CdTe QDs was measured according to the method described earlier.[29] R6G (ethanol as solvent) was chosen as a reference standard (QY = 95%), and zeta potential measurements were performed using a Zetasizer NanoZS90 (Malvern Instruments). Due to the uncertainties of zeta potential measurements, each sample was measured five times and the average data are presented.

2.4. Nonspecifically Binding of QDs with BSA. 100 nM of QD solution was incubated with 100 nM of BSA in PBS to test the nonspecific binding of QDs with BSA. The reactions were carried out at room temperature for 3 h. The mixtures were diluted to a concentration of 10 nM with PBS before FCS measurements, and a two-component fitting procedure was used to measure the percentage of bound QDs with BSA.[25]

2.5. Cell Culture. The A-427 cell line was maintained at 37 °C in a humidified atmosphere containing 5% CO2 in Eagle's Minimal Essential Medium (EMEM) (ATCC) containing 10 μM HEPES, 0.5 μg/mL G418, 100 IU/mL penicillin,100 μg/mL streptomycin, and 10% fetal bovine serum. The growth medium was changed every 2 days until the time of use. After reaching near 80% confluence, cells were dislodged by using 0.05% trypsin, containing 0.02% EDTA.

2.6. Cellular Uptake of Aqueous QDs. For uptake studies of QDs in living cells, cells were seeded onto a sterilized No. 1 coverslip (VWR International, Batavia, IL) inside a 12-well plate and incubated for 24 h before treatment with QDs, unless otherwise stated. After removal of the medium, cells were incubated with QDs at a concentration of 10 nM in 2 mL of PBS for 1 h and washed with PBS three times before measurements. For the 3 h incubation experiment, 10 nM of QDs were incubated with cells for 1 h and the cells were washed with PBS and incubation continued in PBS for another 2 h.

2.7. Confocal Fluorescence Lifetime Imaging Instrumentation. Confocal fluorescence lifetime imaging (FLIM) and FCS measurement were performed using the scanning confocal time-resolved microscopy (Microtime 200, Picoquant GmbH, Germany). 465 nm picosecond pulse lasers were used to excite the QDs. The laser beam was delivered to the samples through an apochromatic 60×/1.2 NA water-immersion objective (Olympus, Japan), and the emitted fluorescence was collected by the same objective and separated from the excitation beam by a dual band dichroic (z467/638rpc, Chroma, VT). A 50 μm pinhole was used to reject the off-focus photons from the excitation volume, and the overall fluorescence was filtered by emission filters (610DF60, Omega Optical, VT) before being detected by a single photon avalanche photodiode (SPAD) (SPCM-AQR, PerkinElmer Inc., Canada). Fluorescence was measured in the time-correlated single photon counting (TCSPC) time-tagged

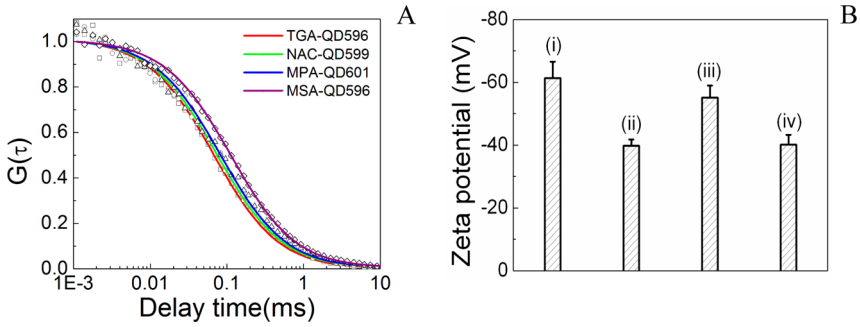

Figure 1. Characterization of different QDs. (A) Normalized FCS curves of TGA-QD596 (i), NAC-QD599 (ii), MPA-QD601 (iii), and MSA-QD596 (iv) in PBS buffer. (B) Zeta potential histogram of QDs determined by Zetasizer.

time-resolved (TTTR) mode (Time Harp200, PicoQuant GmbH, Germany).[23−25]

2.8. Data Analysis for FCS. In FCS, the autocorrelation function $G(\tau)$ is defined as

$$G(\tau) = \frac{\langle \delta F(t)\delta F(t+\tau)\rangle}{\langle F(t)\rangle^2} \quad (1)$$

where the angular brackets represent a time average, $\delta F(t)$ the fluorescence intensity fluctuation at a given time t, and $\delta F(t+\tau)$ fluorescence intensity fluctuations at a time $t+\tau$. The theory of FCS had been described elsewhere.[30,31] When particles diffuse freely in a focal volume with a three-dimensional Gaussian profile, eq 1 can be expressed as[32]

$$G(\tau) = \frac{1}{N}\cdot\frac{1}{1+\frac{\tau}{\tau_D}}\cdot\frac{1}{\sqrt{1+\left(\frac{\omega_0}{z_0}\right)^2\cdot\frac{\tau}{\tau_D}}} \quad (2)$$

Here N is the average number of fluorescent particles in the detection volume, ω_0 and z_0 are lateral and axial radii of the detection volume, and τ_D is the characteristic diffusion time, i.e., the average time the fluorescent molecules reside in the detection volume, where $\tau_D = {\omega_0}^2/4D$, where D is its diffusion coefficient. The effective confocal detection volume (V_{eff}) can be calibrated using aqueous solutions of rhodamine 123 as reference dyes based on the measured structure parameters ($V_{eff} = \pi^{3/2}{\omega_0}^2 z_0$).

For spherical particles, D is inversely proportional to its hydrodynamic diameter (d_H) according to the Stokes−Einstein equation.

$$D = \frac{kT}{3\pi\eta d_H} \quad (3)$$

Here kT is the thermal energy and η is the viscosity. The hydrodynamic diameter, d, of the nanoparticles can be obtained on the basis of the measured characteristic diffusion time of particles (τ_D) and the lateral radius (ω_0) of volume according to eq 4.

$$d_H = \frac{4kT\tau_D}{3\pi\eta{\omega_0}^2} \quad (4)$$

The brightness per particle (BPP) of QDs is a parameter that directly reflects its capacity to emit photons.[33] It can be calculated by dividing the average fluctuating fluorescence signal (count rate) by the average number of QDs (N) in the detection volume.

Two-Component Fitting. When QDs are mixed with BSA, QDs can bind with BSA due to their electrostatic or hydrophobic interaction. The diffusion of free QDs and QD−BSA complex mixture can be represented by the two-component diffusion model given by eq 5 as

$$G(\tau) = \frac{1}{N}\cdot\left(\frac{1-y}{\left(1+\frac{\tau}{\tau_{D1}}\right)}\cdot\frac{1}{\sqrt{1+\left(\frac{\omega_0}{z_0}\right)^2\cdot\frac{\tau}{\tau_{D1}}}} + \frac{y}{\left(1+\frac{\tau}{\tau_{D2}}\right)}\cdot\frac{1}{\sqrt{1+\left(\frac{\omega_0}{z_0}\right)^2\cdot\frac{\tau}{\tau_{D2}}}}\right) \quad (5)$$

where τ_{D1} and τ_{D2} are the diffusion time of free and BSA bound QDs, respectively, and y is the fraction of bound QDs.[25]

MEMFCS Analysis. When QDs are bound to the cell membrane and internalized by cells, single-component fitting or two-component fitting procedure cannot accurately describe the diffusion of QDs in the cells because of the complexity of the cell membrane and diffusion characteristics. MEMFCS is a multicomponent fitting model based on minimizing χ^2 as well as maximizing entropy to obtain an optimal fit in heterogeneous systems. Unlike the conventional single-component fitting or two-component fitting procedure, which fits different diffusion components given a priori, MEMFCS yields the diffusion time distribution instead of a discrete value. MEMFCS has been proven to be a useful tool in studying multicomponent diffusers in a complex system as cells. More information can be found in the refs 25, 34, and 35.

3. RESULTS AND DISCUSSION

3.1. Surface Structure of Thiol-Capped QDs. The surface ligands of aqueous QDs play a vital role in determining their surface structure including the hydrodynamic size, surface ligand density, and surface charge. Here FCS was used to characterize the hydrodynamic size of aqueous QDs.[33,36] Figure 1A shows the normalized FCS curves of different thiol-capped CdTe QDs in PBS that possess almost identical exciton absorption and emission spectra (Figure S-2, Supporting Information). It was observed that their correlation curves shifted right in the order of TGA-, NAC-, MPA-, and MSA-capped CdTe QDs (Figure 1A). The increasing diffusion times show that their hydrodynamic diameter (d_H) increases in the respective order of TGA-, NAC-, MPA-, and MSA-capped CdTe QDs according to eq 4. The exciton absorption and emission spectra of QDs are determined by their size and the

dx.doi.org/10.1021/jp305563p | J. Phys. Chem. B 2012, 116, 12125−12132

lattice structure of the hard core. QDs with similar spectra (Figure S-1, Supporting Information) should have the same size as the hard core, although different ligands may have been used in the synthesis. Hence, the difference in hydrodynamic diameter (d_H) could be attributed to the thicknesses of the soft shell (δ_s) formed by different surface ligands.

Table S1 (Supporting Information) shows the hydrodynamic diameters of CdTe QDs with different PL emission wavelengths. Calculations show that the hydrodynamic diameter (eq 4) increases with their PL emission wavelengths. These values were found to be slightly greater than the measured TEM values (by about 1−2 nm).[37] Of the QDs studied, the MSA-capped QDs had thicker soft ligand layers compared to the others.

Quantitative measurement of the surface composition of QDs by XPS was used to compare the surface ligand density of TGA-QD596, MPA-QD601, MSA-QD596, and NAC-QD599. Experiments show that the surface composition is different for different QDs (Table 1). Quantitative measurement of S and Cd atomic concentration (con %) are based on the spectra of S 2p and Cd 3d, which correspond to binding energies of 405.6 and 162.8 eV, respectively. S is from the thiol ligands bound to the surface of QDs, and Cd is from the hard core of QDs. The size of the hard core for the four QDs used in this study was the same due to their same exciton absorption wavelength; hence, their intrinsic components might be similar. Therefore, the S/Cd ratios actually reflect the ligand binding condition at the surface. Table 1 shows that the TGA-capped QDs have a higher S/Cd ratio and MSA- and NAC-capped QDs have a lower S/Cd ratio. The result suggested that a greater number of thiol ligand molecules was bound or a higher density of surface ligand layers was formed at the surface of TGA-capped QDs compared with other thiol-capped QDs. However, it is difficult to explain the complex reasons that contribute to this difference in surface ligand thickness and density. Potential factors contributing to this difference are the nature of thiols and their integration with the QD surface during the synthesis reaction such as the effect of steric hindrance and bond forces between the ligands and QDs.

Table 1. Quantitative Assessment of the Surface Composition of Aqueous QDs by XPS

QDs	atomic con % (S)	atomic con % (Cd)	S/Cd
TGA-QD596	7.87	9.48	0.830
MPA-QD601	9.00	10.95	0.822
MSA-QD596	7.07	9.46	0.747
NAC-QD599	7.63	10.53	0.725

Some properties of QDs are influenced by the difference in their surface structure. Figure 1B shows the measure of the zeta potential of aqueous QDs. The zeta potentials of all the QDs were found to be less than −30 mV, which indicates that the QDs can be stable in aqueous solution due to their strong electrostatic repulsion. However, significant differences in the zeta potential of the four QDs were noted. For example, the zeta potential of TGA-capped QDs was found to be much lower than that of NAC- and MSA-capped QDs. In nanoparticles, the surface ligand density is a main factor in determining the surface charge of QDs. Obviously, TGA-capped QDs possess higher surface charges primarily due to the larger surface ligand density compared to other QDs. In the following experiments, we assess the role of the surface structure on the photostability of aqueous QDs. Figure S-4 (Supporting Information) shows the photostability of different thiol-capped QDs upon laser excitation. After 600 s of continuous laser irradiation, TGA-QD596 held their fluorescence while the NAC-QD599 and MSA-QD596 lost about 60% of their fluorescence. Our study indicates that TGA-capped QDs have the best photostability among the QDs tested, which agrees with the results of a previous study which shows that the higher surface ligand density on QDs will prevent fluorescence quenching possible from dissolved oxygen due to the shielding effect.[38] In general, the above results suggest that the surface of various aqueous QDs can remarkably be affected by the surface ligands used in the synthesis procedure.

3.2. The Concentration of QDs on Cell Membrane. In consideration of the effect of different ligands on the surface structure of QDs and the reported results on the effect of surface properties of other nanoparticles on their cellular delivery,[39] experiments and information on the possible effect of the surface structure of QDs on cellular uptake has not been investigated. Here we examine the distribution of various QDs

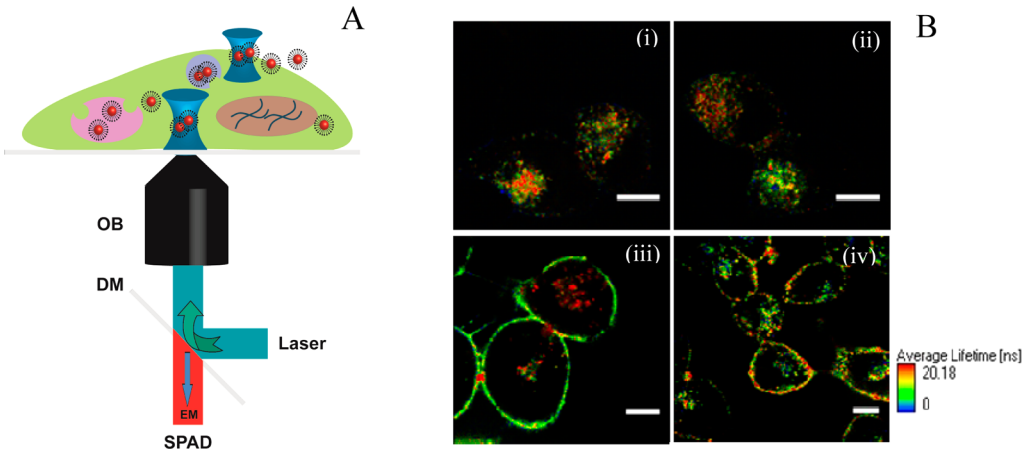

Figure 2. (A) Schematic representation of concentration and diffusion assessment of QDs in living cells using a confocal FCS system. OB: water-immersion objective (60×/1.2 NA). DM: dichroic mirror (z467/638rpc). SPAD: single photon avalanche photodiode. (B) Confocal fluorescence lifetime imaging of different QDs in living cells. A-427 cells were incubated with 10 nM of TGA-QD596 (i), NAC-QD599 (ii), MPA-QD601 (iii), and MSA-QD596 (iv) in PBS for 1 h. It was excited with a 465 nm laser. Scale bars = 10 μm.

dx.doi.org/10.1021/jp305563p | J. Phys. Chem. B 2012, 116, 12125−12132

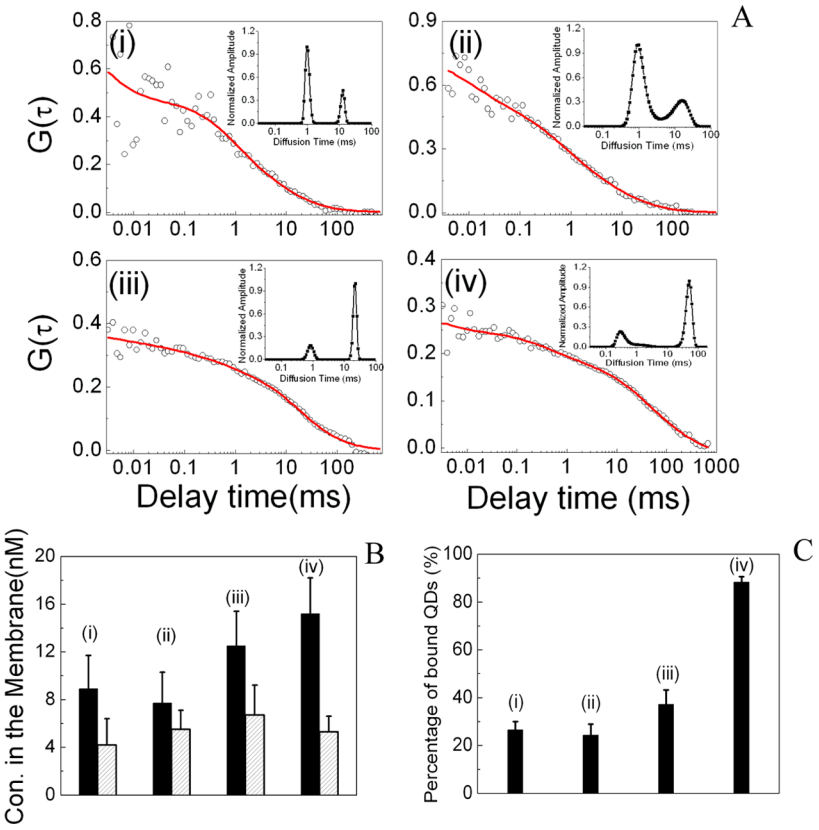

Figure 3. FCS measurements and diffusion behavior analysis of QDs in the membrane using MEMFCS software. (A) Typical autocorrelation curves of TGA-QD596 (i), NAC-QD599 (ii), MPA-QD601 (iii), and MSA-QD596 (iv) in the membrane and their corresponding fitted curves using MEMFCS (red solid lines). Insets are a continuous distribution of diffusion time of QDs in the membrane analyzed by MEMFCS. (B) The concentration distribution of QDs in the membrane measured based on $G(0)$ values in the autocorrelation curves. The incubation times are 1 h (black) and 3 h (bias), respectively. (C) The percentage of bound QDs with BSA measured with a two-component fitting procedure when 100 nM of QDs was reacted with the same concentration of BSA in PBS for 3 h.

uptaken by live cells under physiological conditions using FCS and MEMFCS (Figure 2A). It was found that QDs with different functionality exhibit different adsorption and internalization characteristics. Diffusion characteristics are measured by FCS, where the amplitude of autocorrelation curves ($G(0)$), which is inversely proportional to the average number (N) of QDs in the effective detection volume (V_{eff}), is obtained by monitoring fluorescence fluctuations in a diffraction limited focused spot. The concentration (C) can then be calculated by dividing N by V_{eff} ($C = N/(N_A{*}V_{eff})$), where N_A is the Avogadro constant. The concentration of QDs in different compartments or locations in a cell can then be determined by focusing the laser beam at a specific spot of interest.[35,40] Figure 2B shows the confocal fluorescence lifetime images of TGA-QD596, NAC-QD599, MPA-QD601, and MSA-QD596 incubated with A-427 cells for 1 h. On one hand, high uptake efficiency of QDs was noted as evident from the discrete bright spots in the cytoplasm by directly focusing in the cytosol, although they were not modified with any antibodies or peptides that can specifically recognize the receptors at the cell surface. It has been reported that bare QDs with carboxylic acid surface coating can be internalized by the early endosomes and then transferred to late endosomes or lysosomes after being recognized by lipid rafts.[41] On the other hand, it is clear that MPA-QD601 and MSA-QD596 were bound to the membrane to a greater extent compared to TGA-QD596 and NAC-QD599 based on their stronger membrane PL signifying their higher affinity to the plasma membrane of cells compared with TGA- and NAC-capped QDs. Our study suggests different interactions between QDs and cells during their uptake.

Figure 3A presents a typical autocorrelation curve of QD diffusion obtained by focusing the laser at the membrane. Due to QDs' interaction with cell membrane and heterogeneity of the cell membrane, the autocorrelation curves reflect the complex of various diffusion behaviors of QDs in the membrane, including free diffusion, anomalous diffusion, and restricted diffusion among others. MEMFCS has been successfully used to assess the complex diffusion dynamics of nanoparticles in the cells.[25,34,35] Different from the conventional fitting procedure, MEMFCS can provide a distribution of different diffusion times whereby species diffusing at different rates can be monitored by a single analysis, as shown in the inset of Figure 3A. Two peaks corresponding to the diffusion time distribution of QDs in the cell membrane can be noted. The faster diffusers (the first peak) could be attributed to the diffusion of unbound QDs at the membrane. The slower diffusers (the second peak) are due to the lower mobility of the QD complex in the membrane possibly due to the strong affinity of membrane proteins to QDs.

Meanwhile, it is very important to note that the difference in amplitude ($G(0)$) in the FCS curves directly reflects the effect of the surface structure of the thiol-capped QDs upon interacting with the cell membrane. Measurements reported in Figure 3B are the average from more than 10 cells using single point FCS by directly focusing at the membrane. Experiments show that, when 10 nM of QDs were incubated

dx.doi.org/10.1021/jp305563p | J. Phys. Chem. B 2012, 116, 12125−12132

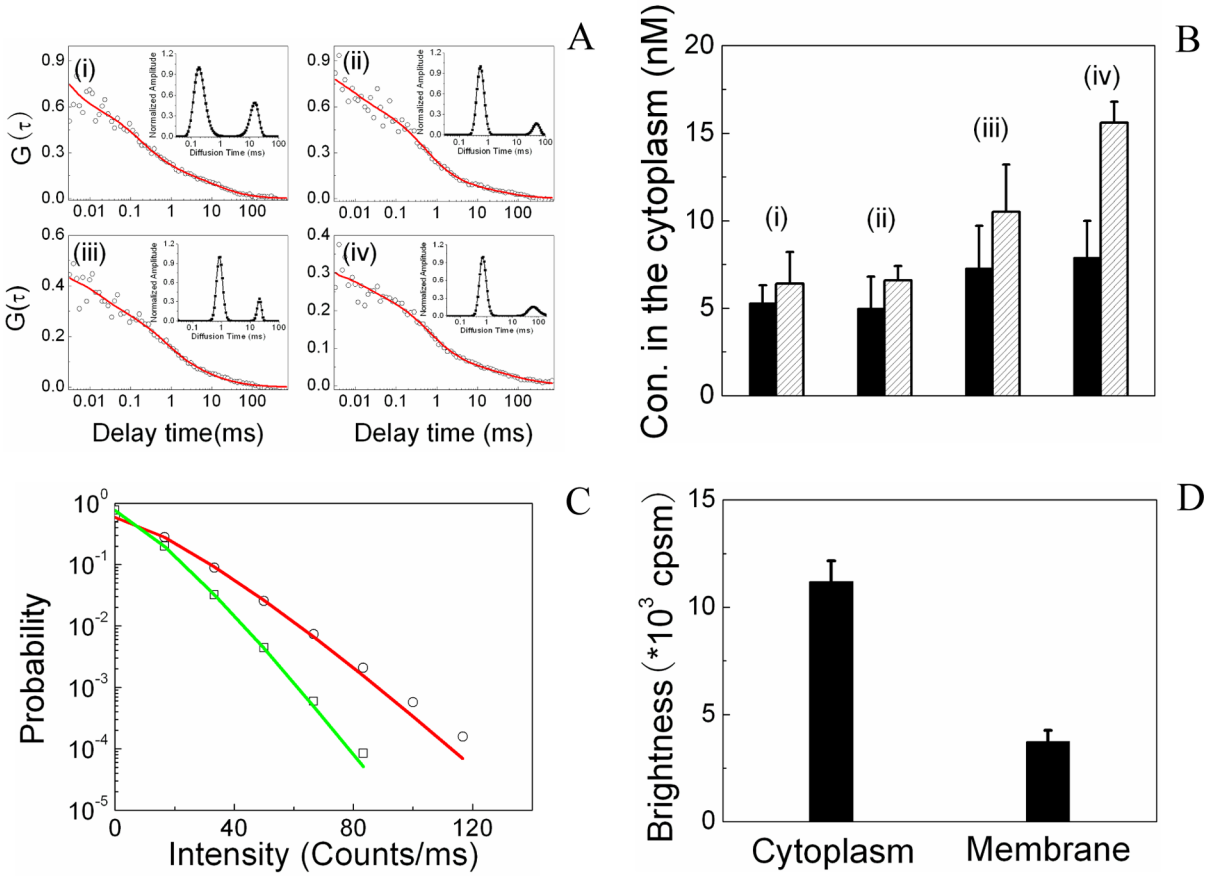

Figure 4. FCS measurements and diffusion dynamics analysis of QDs in the cytoplasm by MEMFCS software. (A) Typical autocorrelation curves of TGA-QD596 (i), NAC-QD599 (ii), MPA-QD601 (iii), and MSA-QD596 (iv) in the cytosol and the corresponding fitted curves by MEMFCS (red solid lines). QDs were incubated with cells for 3 h. Insets are a continuous distribution of diffusion time of QDs in the cytoplasm by MEMFCS. (B) The concentration distribution of QDs in the cytoplasm measured after 1 h (black) and 3 h (bias) of incubation. (C) Photon counting histogram (PCH) analysis of MPA-QD601 bound to the membrane (open squares) and accumulation in the cytoplasm (open circles) based on the obtained fluorescence fluctuation data. Single component (i = 1, χ^2 = 1.65) fitting (solid lines) is shown. (D) Calculated brightness of MPA-QD601 from PCH analysis. Error bars denote standard deviation (n = 10).

with cells for 1 h, the concentration of the respective bound population at the surface was in the range between 5 and 20 nM. Upon comparison, the concentration of MSA-capped QDs at the membrane was found to be much higher than the TGA- and NAC-capped QDs. When the incubation time was increased to 3 h, the concentration of QDs at the membrane decreased as expected due to internalization by cells.

The difference in the concentration of QDs bound to the membrane could be related to the interaction and affinity of the thiol-capped QDs with the membrane proteins. When choosing BSA as a protein model to test its interaction, the four QDs tested showed different affinities to BSA (Figure 3C). The striking result with the two-component fitting procedure is that the percentage of MSA-capped QDs bound with BSA was the largest and that of TGA- or NAC-capped QDs with BSA was the least. The strong affinity of MSA-capped QDs on BSA is possibly due to the lower electrostatic repulsion effect between BSA- and MSA-capped QDs, as determined by its lower surface zeta potential value (Figure 1B). As we know, internalization of QDs by living cells consists of two phases: an initial binding phase to the plasma membrane of cells, followed by a gradual internalization. The MSA-capping on QDs yields a bigger surface contact area with membrane protein and a relatively neutral surface potential and hence can interact with the negatively charged membrane more strongly compared to their counterparts. These results indicate that the interaction between the plasma membrane and QDs with different surface structure directly influences the cellular delivery and subcellular distribution of QDs.

3.3. Cellular Uptake of Aqueous QDs as a Function of Their Hydrodynamic Diameter. First, it was verified that a majority of QDs were free in the cytosol and not localized in the organelles from the results of MEMFCS analysis. Figure 4A presents typical FCS curves of QDs in the intracellular compartments obtained when a laser (465 nm) was focused into the cells. Meanwhile, MEMFCS was used to assess the diffusion dynamics of QDs in the intracellular regions and assess their localization in cells. The inset of Figure 4A is the obtained continuous distribution of diffusion time of QDs in the cytoplasm by fitting the autocorrelation curves in Figure 4A with MEMFCS. Two peaks indicate that there are two different diffusion behaviors of QDs in the intracellular space but the faster component absolutely dominates over that of the slower.[34] The diffusion time of the faster component was within several hundred microseconds. Figure S-4 (Supporting Information) is the diffusion time distribution of the four QDs in PBS buffer (on control), and their average diffusion times were about 0.1 ms. Taking into account the influence of viscosity of the fluid phase in the cytosol on the diffusion time (which is approximately 4 times the viscosity of water),[42] the

dx.doi.org/10.1021/jp305563p | J. Phys. Chem. B 2012, 116, 12125−12132

faster component should be from the freely diffusing QDs in the cytosol (inset of Figure 4A). The diffusion time of the slower component is in the range of 10 and 100 ms that could be attributed to the low mobility of the QD complex in the organelles, possibly the endosome and lysosome. Our results are consistent with the existing data of the diffusion of nanoparticles in these two cellular organelles in the cytosol.[25] The most important result of all, the absolute domination of the faster component over the slower one, suggests that the freely diffusing QDs are mainly from the cytosol, possibly demonstrating that aqueous QDs might have the potential to escape trapped environments to accumulate in the cytoplasm. Our results support the findings by Nabiev et al. that aqueous QDs can further penetrate the endosome and enter the cytoplasm after they accumulate in the endosome along microtubules.[43]

Second, it was found that the internalization of aqueous QDs was highly dependent on its hydrodynamic diameter but is less influenced by its surface charge. From the data presented in Table S-1 (Supporting Information) and Figure 1B, we note that there is a big difference in the zeta potential between NAC-QD599 and TGA-QD596 but a minor difference in the hydrodynamic diameter. However, after internalization, their intracellular concentration was almost identical, as shown in Figure 4B even after 3 h of incubation. However, a significant difference in the uptake was also noted between NAC-QD599 and MSA-QD596. Here, MSA-QD596 had a greater hydrodynamic diameter compared to NAC-QD599 but less difference in their zeta potential. Figure 4B shows that the higher concentration of MSA-QD596 accumulated in the intracellular compartments compared with NAC-QD599 and the difference was more pronounced when the incubation time increased to 3 h. It should also be pointed out that the size of the QD's hardcore was almost identical, suggesting that the cellular uptake of small size QDs can be dramatically determined by their hydrodynamic diameter and is not directly related to their surface charges.

Similar phenomena on the cellular uptake of gold nanoparticles were reported by Chan et al. The authors noted that cellular uptake of gold nanoparticles is vastly size-dependent (of hardcore) in the range of 10 and 50 nm. Possible reasons speculated are the curvature difference posed by nanoparticles with different sizes.[15] The absorption characteristics of different sizes of NAC-capped QDs by the cell membrane was explored. Figure S-5 (Supporting Information) is a typical autocorrelation profile of NAC-capped QD580 (d_H: ~2.5 nm) and QD680 (d_H: ~6.5 nm) obtained from one identical laser focus point in the membrane when 10 nM of QD580 and QD680 were coincubated with A-427 cells in PBS for 2 h. The amplitudes in the autocorrelations show that more QD680 were bound than QD580 in the cell membrane. The concentration difference suggests that binding of QDs in the membrane is directly related to the size of QDs and bigger size QDs have stronger affinity to the membrane. Zhang et al. demonstrated that the uptake mechanism of QDs is primarily via the G-protein-coupled receptor associated pathway and low-density lipoprotein receptor/scavenger receptor-mediated endocytosis.[41] Hence, we speculate that, with the cellular uptake of aqueous QDs mediated by receptors in the cell membrane, QDs with larger hydrodynamic diameter have a larger surface contact area with the cell-surface lipid bilayers which facilitates internalization. Another reason could be due to the lower density of surface ligands for MSA-capped QDs. As shown in Figure 3C, serum proteins can more efficiently interact with MSA-capped QDs due to its lower surface ligand coverage. Different from other nanoparticles such as gold nanoparticles (>10 nm), hydrodynamic sizes of aqueous QDs (<10 nm) are of the same order as the proteins in the cells and even less if their surface ligand layer is stripped. The force and interfacial phenomena between QDs and cell membrane would affect the uptake of aqueous QDs. However, more studies are required.[44]

Finally, photon counting histogram (PCH) analysis at the membrane and cytoplasm (Figure 4C) can provide further insight on the internalization process of QDs. As seen from Figure 2C, MPA-capped QDs exhibit different lifetime distributions upon localizing in different regions within the cells. A relatively lower fluorescence lifetime was noted at the membrane (green color) compared with that in the cytoplasm (red color). A likely reason could be the ongoing energy transfer from QDs to the proteins in the membrane upon binding. PCH analysis (Figure 4D) shows that the brightness of QDs in the cytoplasm is 3 times higher than that in the membrane. It is known that, after QDs traffic through the vesicles to acidic environments (pH 4.5), they readily aggregate, which results in a decrease in fluorescence intensity due to the acidic environment.[45] Nabiev et al. demonstrated that the surface protonation of CdTe QDs in the endosomal and lysosomal compartments and the resulting reversible and pH-dependent aggregation of QDs could be the primary reason for their escape from the endosome into the cytoplasm.[43] The PCH result demonstrates that, when QDs penetrate the membrane barrier, they escape from the trapped environments and reorganize in the cytosol, as noted from the recovery of fluorescence intensity. The above results suggest that aqueous QDs are mobile and have the potential to escape from trapped environments (potentially endosomes and lysosomes) and accumulate or reorganize in the cytosol. Although our experiments are in line with the previous findings, time course experiments need to be conducted to quantify the QDs in the different compartments simultaneously.

4. CONCLUSIONS

The surface structure of aqueous QDs is very different compared to that of bigger size nanoparticles (10−100 nm). They are greatly dominated by the relatively thicker surface ligand layer, exterior hydration layer, and small size of the hardcore. Capping of QDs with different ligands yields particles with remarkably different surface ligand thickness, ligand density, and zeta potential, that can possibly affect their optical properties and interaction with cells, which affect its uptake and trafficking. FCS is an effective tool to measure the concentration and dynamics of QDs in live cells. Quantitative analyses based on FCS and MEMFCS show that bare aqueous QDs can easily be internalized by the cells to accumulate in the cytoplasm. Quantities of various QDs absorbed to the cell membrane are affected by their interaction kinetics. And quantities of internalized QDs in living cells are not influenced by their surface charge but are dependent on their hydrodynamic radius. Given the importance of QDs in live-cell imaging, we expect our findings to provide a basic understanding of their interaction and intracellular localization in live cells.

■ ASSOCIATED CONTENT

Supporting Information

Figures of BPP histogram of QDs, UV−vis absorbance and PL spectra of QDs, and photostability of QDs, continuous diffusion time distribution of QDs in PBS buffer, the autocorrelation curves of QD580 and QD680 in the cell membrane obtained from one identical focus point when the same concentration of QD580 and QD680 was coincubated with cells, and table of hydrodynamic diameter of QDs with different thiol-capping. This material is available free of charge via the Internet at http://pubs.acs.org.

■ AUTHOR INFORMATION

Notes

The authors declare no competing financial interest.

■ ACKNOWLEDGMENTS

This work was partially supported by grants from the Purdue Center for Cancer Research, the Clinical and Translational Sciences Institute, the National Science Foundation (NSF 0945771), and the Indo-US Knowledge Network grant.

■ REFERENCES

(1) Chan, W. C. W.; Nie, S. *Science* **1998**, *281*, 2016−2018.
(2) Bruchez, M., Jr.; Moronne, M.; Gin, P.; Weiss, S.; Alivisatos, A. P. *Science* **1998**, *281*, 2013−2015.
(3) Jaiswal, J. K.; Mattoussi, H.; Mauro, J. M.; Simon, S. M. *Nat. Biotechnol.* **2003**, *21*, 47−51.
(4) Gao, X.; Cui, Y.; Levenson, R. M.; Chung, L. W.; Nie, S. *Nat. Biotechnol.* **2004**, *22*, 969−976.
(5) Samia, A. C. S.; Chen, X.; Burda, C. *J. Am. Chem. Soc.* **2003**, *125*, 15736−15737.
(6) Bakalova, R.; Ohba, H.; Zhelev, Z.; Nagase, T.; Jose, R.; Ishikawa, M.; Baba, Y. *Nano Lett.* **2004**, *4*, 1567−1573.
(7) Choi, H. S; Liu, W.; Misra, P.; Tanaka, E.; Zimmer, J. P.; Itty Ipe, B.; Bawendi, M. G.; Frangioni, J. V. *Nat. Biotechnol.* **2007**, *25*, 1165−1170.
(8) Howarth, M.; Liu, W.; Puthenveetil, S.; Zheng, Y.; Marshall, L. F.; Schmidt, M. M.; Wittrup, K. D.; Bawendi, M. G.; Ting, A. Y. *Nat. Methods* **2008**, *5*, 397−399.
(9) Park, J.; Nam, J.; Won, N.; Jin, H.; Jung, S.; Jung, S.; Cho, S.; Kim, S. *Adv. Funct. Mater.* **2011**, *21*, 1558−1566.
(10) Barua, S.; Rege, K. *Small* **2009**, *5*, 370−376.
(11) Rogach, A. L.; Franzl, T.; Klar, T. A.; Feldmann, J.; Gaponik, N.; Lesnyak, V.; Shavel, A.; Eychmuller, A.; Rakovich, Y. P.; Donegan, J. F. *J. Phys. Chem. C* **2007**, *111*, 14628−14637.
(12) Conroy, J.; Byrne, S. J.; Gun'ko, Y. K.; Rakovich, Y. P.; Donegan, J. F.; Davies, A.; Kelleher, D.; Volkov, Y. *Small* **2008**, *4*, 2006−2015.
(13) Ryman-Rasmussen, J. P.; Riviere, J. E.; Monteiro-Riviere, N. A. *Nano Lett.* **2007**, *7*, 1344−1348.
(14) Zhang, Y.; Mi, L.; Xiong, R.; Wang, P.; Chen, J.; Yang, W.; Wang, C.; Peng, Q. *Nanoscale Res. Lett.* **2009**, *4*, 606−612.
(15) Chithrani, B. D.; Ghazani, A. A.; Chan, W. C. W. *Nano Lett.* **2006**, *6*, 662−668.
(16) Jiang, W.; Kim, B. Y. S.; Rutka, J. T.; Chan, W. C. W. *Nat. Nanotechnol.* **2008**, *3*, 145−150.
(17) Cho, E. C.; Xie, J.; Wurm, P. A.; Xia, Y. *Nano Lett* **2009**, *9*, 1080−1084.
(18) Zhu, Z. J.; Yeh, Y. C.; Tang, R.; Yan, B.; Tamayo, J.; Vachet, R. W.; Rotello, V. M. *Nat. Chem.* **2011**, *3*, 963−968.
(19) Dong, C. Q.; Ren, J. C. *Analyst* **2010**, *135*, 1395−1399.
(20) Rigler, R.; Mets, U.; Widengren, J.; Kask, P. *Eur. Biophys. J.* **1993**, *22*, 169−175.
(21) Schwille, P.; Haupts, U.; Maiti, S.; Webb, W. W. *Biophys. J.* **1999**, *77*, 2251−2265.
(22) Kannan, B.; Har, J. Y.; Liu, P.; Maruyama, I.; Ding, J. L.; Wohland, T. *Anal. Chem.* **2006**, *78*, 3444−3451.
(23) Varghese, L.; Sinha, R.; Irudayaraj, J. *Anal. Chim. Acta* **2008**, *625*, 103−109.
(24) Chen, J.; Wang, C.; Irudayaraj, J. *J. Biomed. Opt.* **2009**, *14*, 040501.
(25) Chen, J.; Irudayaraj, J. *ACS Nano* **2009**, *3*, 4071−4079.
(26) Wang, Y.; Chen, J.; Irudayaraj, J. *ACS Nano* **2011**, *5*, 9718−9725.
(27) Wang, C.; Chen, J.; Talavange, T.; Irudayaraj, J. *Angew. Chem., Int. Ed.* **2009**, *121*, 2797−2801.
(28) Zhang, H.; Wang, L. P.; Xiong, H. M.; Hu, L. H.; Yang, B.; Li, W. *Adv. Mater.* **2003**, *15*, 1712−1715.
(29) Li, L.; Qian, H.; Ren, J. *Chem. Commun.* **2005**, *4*, 528−530.
(30) Magde, D.; Elson, E.; Webb, W. W. *Phys. Rev. Lett.* **1972**, *29*, 705−708.
(31) Elson, E.; Madge, D. *Biopolymers* **1974**, *13*, 1−27.
(32) Aragón, S. R.; Pecora, R. *J. Chem. Phys.* **1976**, *64*, 1791−1803.
(33) Doose, S.; Tsay, J.; Pinaud, F.; Weiss, S. *Anal. Chem.* **2005**, *77*, 2235−2242.
(34) Sengupta, P.; Garai, K.; Balaji, J.; Periasamy, N.; Maiti, S. *Biophys. J.* **2003**, *84*, 1977−1984.
(35) Chen, J.; Nag, S.; Vidi, P.; Irudayaraj, J. *PLoS ONE* **2011**, *6*, e17991.
(36) Dong, C. Q.; Bi, R.; Qian, H. F.; Li, L.; Ren, J. C. *Small* **2006**, *2*, 534−538.
(37) Yu, W. W.; Qu, L.; Guo, W.; Peng, X. *Chem. Mater.* **2003**, *15*, 2854−2860.
(38) Aldana, J.; Wang, Y.; Peng, X. *J. Am. Chem. Soc.* **2001**, *123*, 8844−8850.
(39) Verma, A.; Stellacci, F. *Small* **2010**, *6*, 12−21.
(40) Nag, S.; Chen, J.; Maiti, S.; Irudayaraj, J. *Biophys. J.* **2010**, *99*, 1969−1975.
(41) Zhang, L. W.; Monteiro-Riviere, N. A. *Toxicol. Sci.* **2009**, *110*, 138−155.
(42) Verkman, A. S. *Trends Biochem. Sci.* **2002**, *27*, 27−33.
(43) Nabiev, I.; Mitche, S.; Davies, A.; Williams, Y.; Kelleher, D.; Moore, R.; Gun'ko, Y. K.; Byrne, S.; Rakovich, Y. P.; Donegan, J. F.; et al. *Nano Lett.* **2007**, *7*, 3452−3461.
(44) Nel, A. E.; Mädler, l.; Velegol, D.; Xia, T.; Hoek, E.M. V.; Somasundaran, P.; Klaessig, F.; Castranova, V.; Thompson, M. *Nat. Mater.* **2009**, *8*, 543−557.
(45) Zhang, H.; Zhou, Z.; Yang, B.; Gao, M. Y. *J. Phys. Chem. B* **2003**, *107*, 8−13.